THE JOURNAL OF PHYSICAL CHEMISTRY LETTERS
A JOURNAL OF THE AMERICAN CHEMICAL SOCIETY

pubs.acs.org/JPCL

Letter

Solid-State Alder-Ene Reaction of 1-Hexene under High Pressure

Jingqin Xu, Puyi Lang, Shijie Liang, Jie Zhang, Yunfan Fei, Yajie Wang, Dexiang Gao, Takanori Hattori, Jun Abe, Xiao Dong, Haiyan Zheng, and Kuo Li*

Cite This: *J. Phys. Chem. Lett.* 2025, 16, 2445−2451

Read Online

ACCESS | Metrics & More | Article Recommendations | Supporting Information

ABSTRACT: The Alder-ene reaction is a chemical reaction between an alkene with an allylic hydrogen, and it provides an efficient method to construct the C−C bond. Traditionally, this reaction requires catalysts, high temperatures, or photocatalysis. In this study, we reported a high-pressure-induced solid-state Alder-ene reaction of 1-hexene at room temperature without a catalyst. 1-Hexene crystallizes at 4.3 GPa and polymerizes at 18 GPa, forming olefins. By exploring gas chromatography−mass spectrometry, we discovered that 1-hexene generates dimeric products through the Alder-ene reaction under high pressures. The *in situ* neutron diffraction shows that the reaction process did not obey the topochemical rule. A six-membered ring transition state including one C−H σ bond and two alkene π bonds was evidenced by the theoretical calculation, whose energy obviously decreased when compressed to 20 GPa. Our work offers a novel and promising method to realize the Alder-ene reaction at room temperature without a catalyst, expanding the application of this important reaction.

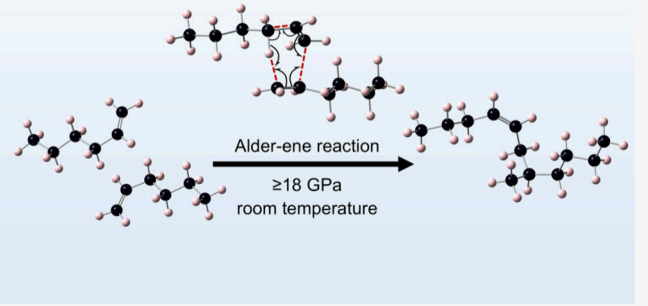

The Alder-ene reaction is a pivotal organic chemical reaction for constructing carbon−carbon bonds. It involves the addition of an alkene π bond and an allylic C−H σ bond known as the ene to an electron-deficient alkene or alkyne (the enophile) via a pericyclic reaction. Consequently, the π bond shifts, and new C−H and C−C σ bonds are formed.[1−4] This reaction is compatible with a broad range of functional groups and has been extended to heteroatom-substituted ene components, making it widely applicable in the synthesis of complex molecules and natural products.[5−8]

The Alder-ene reaction involves the cleavage of an allylic C−H σ bond, which has a high activation energy and usually requires high temperature.[8,9] For example, in the isomeric Alder-ene reaction between ethanimine and ethylene under non-catalyzed conditions, the activation free energy is typically above 198.7 kJ/mol,[8] and high temperature is therefore required. However, high temperature often results in low yields, poor selectivity, and even the reverse reaction, which limits the application of the Alder-ene reaction.[10,11] Much effort has been devoted to develop the catalyst to accelerate the ene reaction and improve the reaction efficiency under relatively mild conditions, like Lewis acid catalysts,[12] metal catalyst[13−17] and organo-[18,19] and bio-[20] catalyzed ene reactions.

High pressure is an effective strategy to compress the intermolecular distance and induce chemical reactions. In contrast to the traditional solution reaction, high-pressure reactions usually take place in the solid state without using the solvent, catalysts, or radical initiators, which can be recognized as a green chemistry process. Recently, a lot of theoretical and experimental studies have demonstrated that high pressure can significantly lower the energy barrier of addition reactions like the Diels−Alder reaction effectively, by compressing the volume of the reactants and transition states.[21] Theoretically, Chen et al. evidenced that the activation energy of the Diels−Alder reaction between cyclopentadiene and ethylene decreases markedly with increasing pressure.[21] Experimentally, a lot of studies have shown that the alkynes and even the very stable aromatic compounds can take part in the Diels−Alder reactions initiated by high pressure. 1,3,5-Triethynylbenzene,[22] 1,4-diphenylbutadiyne,[23] azobenzene,[24] and arylazo[25] can undergo dehydro-Diels−Alder or hetero-Diels−Alder reactions under compression, to produce graphitic nanoribbons. Aromatics, like furan,[26] thiophene,[27] pyridazine,[28] and 2,5-furandicarboxylic acid,[29] also experienced Diels−Alder reactions under high pressure, which becomes the most promising method to prepare the famous diamond nanothread materials. On the other hand, recently, it was reported that the C−H σ bond of the methyl group in 2-butyne can be activated under high pressure, facilitating intermolecular CH···π H transfer. The process contains double H transfer via an aromatic Hückel

Received: December 26, 2024
Revised: February 9, 2025
Accepted: February 24, 2025
Published: February 27, 2025

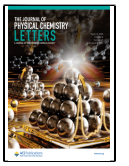

https://doi.org/10.1021/acs.jpclett.4c03696
J. Phys. Chem. Lett. 2025, 16, 2445−2451

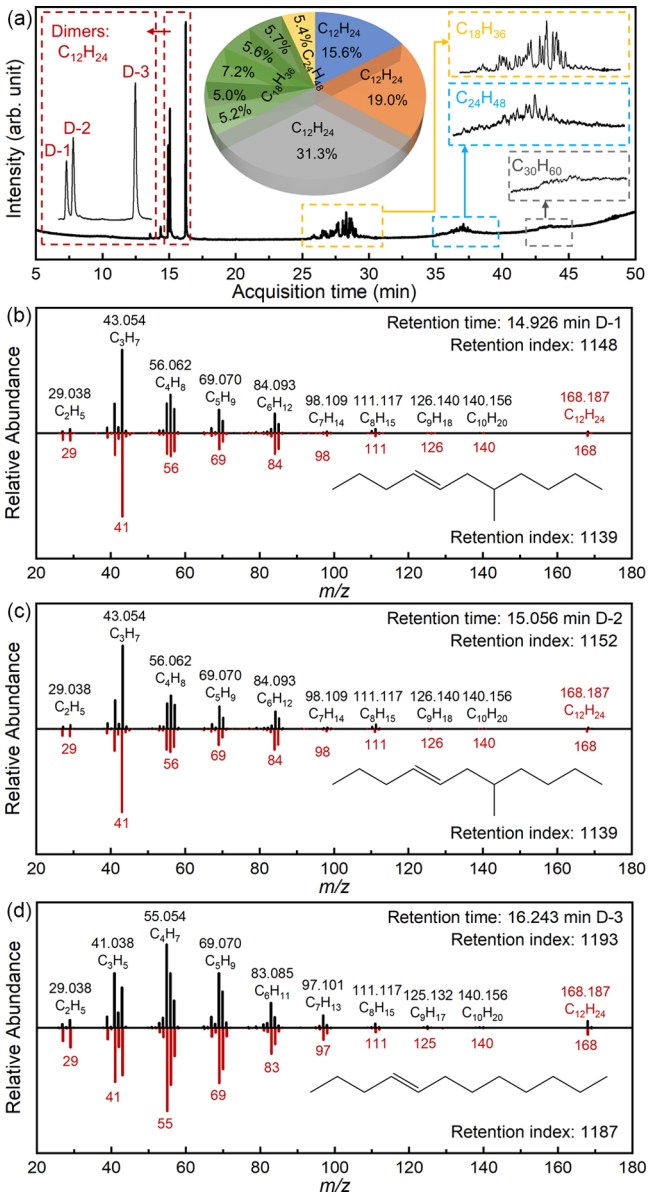

Figure 1. (a) TICs of PE-20. The inset displays the distribution of products with a content higher than 2%. D-1, D-2, and D-3 represent the three isomers of the dimers in PE-20. The retention index and mass spectroscopies of dimers (b) D-1, (c) D-2, and (d) D-3 (black line) are compared to the NIST database (red line).

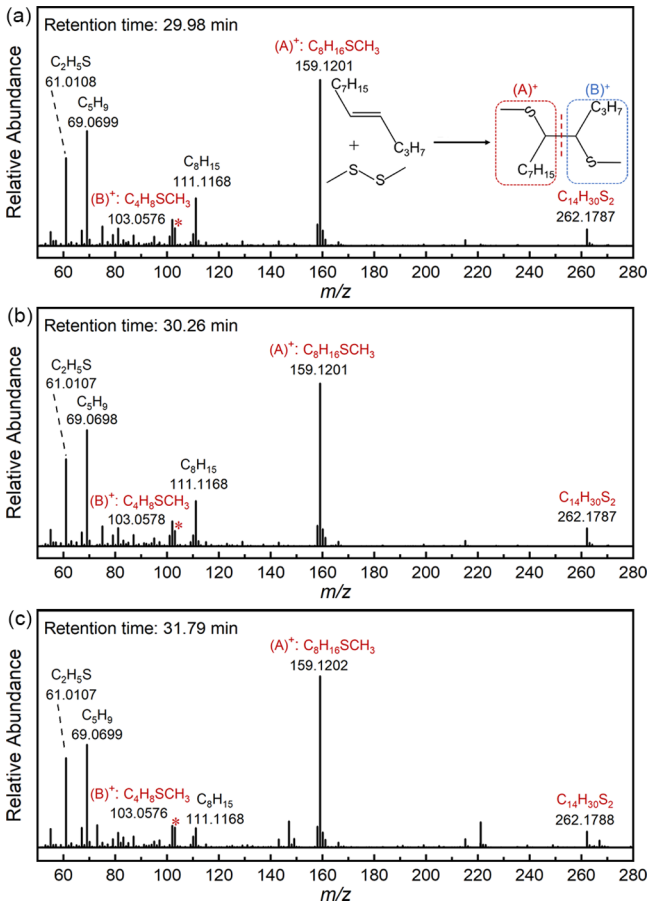

Figure 2. Mass spectrum of the product resulting from the reaction of $C_{12}H_{24}$ with DMDS at the retention times of (a) 29.98 min, (b) 30.26 min, and (c) 31.79 min. The inset illustrates the reaction process of olefine and DMDS.

Scheme 1. Proposed Alder-Ene Reaction Pathway from 1-Hexene to Dimers

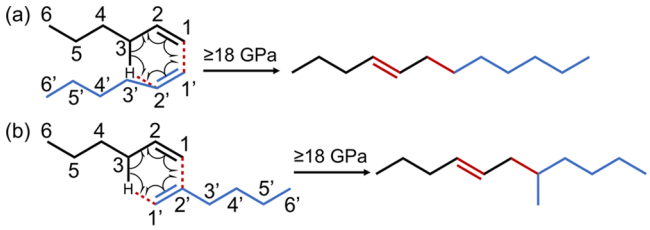

six-membered ring intermediate state, and the energy barrier was significantly reduced by external pressure.[30] This reminds us that the Alder-ene reaction, a pericyclic reaction with an allylic H atom shifting to C═C in alkene, may also be promoted under high pressure. In this study, we investigated the phase transition and chemical reaction process of 1-hexene under high pressure. We found a pressure-driven Alder-ene reaction between 1-hexene molecules. The energy barrier was significantly suppressed to ~60 kJ/mol at 20 GPa, which is key to the reaction. This work discloses a new reaction condition of the Alder-ene reaction and offers new insights into the hydrogen transfer behavior in hydrocarbon systems under extreme conditions.

In situ Raman and infrared (IR) spectroscopy at room temperature (Figures S1−S3 and Table S1 of the Supporting Information) disclosed that 1-hexene crystallizes at 4.2 GPa, which is consistent with refs 31 and 32. Above 18 GPa, all peaks broaden, and the pressure dependence of Raman and IR modes exhibits discontinuity, indicating that hexene begins to react. As shown in Figure S4 of the Supporting Information, with compression to 22.6 GPa and maintenance for 20 h, distinct C═C stretching was observed in the Raman spectra of the product upon decompression to 2.2 GPa, which clearly differs from those of the raw material. The intensity of the peaks associated with the sp^2 C−H stretching of 1-hexene significantly decreased, indicating the transformation of terminal alkenes (C═C) into new internal alkene structures.[31] The conversion ratio was increased obviously when the pressure is increased to 40 GPa, as evidenced by the increased intensity of the new C═C stretching centered at 1662 cm^{-1} (Figure S1 of the Supporting Information).

https://doi.org/10.1021/acs.jpclett.4c03696
J. Phys. Chem. Lett. 2025, 16, 2445−2451

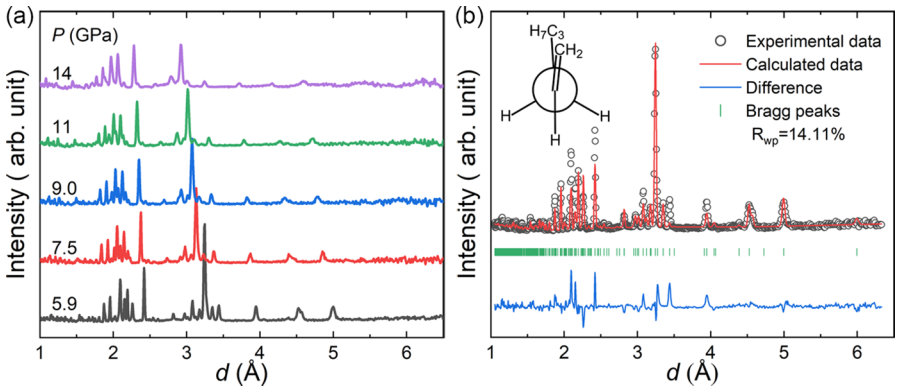

Figure 3. High-pressure neutron diffraction analysis of C_6D_{12}. (a) *In situ* neutron diffraction patterns of C_6D_{12} under high pressure. (b) Rietveld refinement plot of C_6D_{12} at 5.9 GPa.

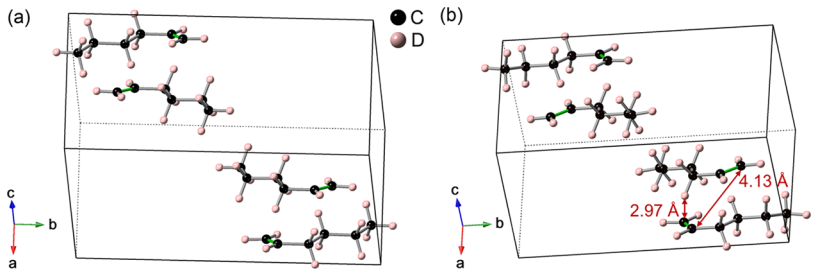

Figure 4. Crystal structure of C_6D_{12} under (a) 5.9 and (b) 18 GPa (optimized by CASTEP). The green bonds represent C═C.

To understand the reaction mechanism, we compressed 1-hexene to 20 GPa using a Paris−Edinburgh press (PE press) and successfully collected the colorless transparent liquid product (PE-20) after decompression. The product was dissolved in dichloromethane, and the oligomers were then analyzed by gas chromatography−mass spectrometry (GC−MS). The total ion chromatogram (TIC) is displayed in Figure 1a. Compounds with concentrations exceeding 2%, including dimeric ($C_{12}H_{24}$), trimeric ($C_{18}H_{36}$) and tetrameric ($C_{24}H_{48}$), were detected. Additionally, trace amounts (<2%) of pentameric ($C_{30}H_{60}$) compounds were observed, with the dimers being the predominant species. All of these molecules exhibit a composition of $(C_6H_{12})_n$, with n as an integer, indicating no loss or addition of hydrogen atoms or carbon fragments. This contrasts sharply with the products of free radical polymerizations, which often gain or lose a radical (such as H•) to terminate the chain reaction.[33] Therefore, we speculate that the pressure-induced polymerization (PIP) of 1-hexene should result from some direct addition reaction including H transfer, like the polymerization process that happened in 2-butyne under high pressure.[30]

Three isomers of the dimer ($C_{12}H_{24}$, D-1, D-2, and D-3) were observed in the TIC plot (Figure 1a) with their MS shown in panels b, c, and d of Figure 1. Referencing the retention index from the National Institute of Standards and Technology (NIST) of linear and branched dodecene and combining their mass spectroscopies (panels b, c, and d of Figure 1 and Table S2 of the Supporting Information), we found that the retention indices of D-1 (1148) and D-2 (1152) are similar to that of 7-methylundec-4-ene (1139). Additionally, the index for D-3 (1193) is close to that of 4-dodecene (1187). Therefore, we conclude that D-1 and D-2 are branched dodecene, and they are probably *cis*−*trans* isomers due to their similar retention time and same mass spectroscopies, while D-3 is identified as a linear aliphatic olefin ($C_{12}H_{24}$).

To locate the double-bond position on the dodecene further, we explored the dimethyl disulfide (DMDS) derivatization approach.[34,35] DMDS was added to the recovered product in hexane solvent, and it reacted with the double bond in the product, as shown in the inset of Figure 2a. Then, the MS was measured under the electron ionization (EI, 70 eV) conditions, and three isomers of $C_{12}H_{24}(CH_3S)_2$ were detected with the retention times at 29.98, 30.26, and 31.79 min, corresponding to the three isomers of $C_{12}H_{24}$ observed in Figure 1a. The double bond was then located easily by recognizing the major fragment ions $(A)^+$ and $(B)^+$, which were formed by cleavage of the carbon−carbon bond between the neighboring methylthio-carbon atoms. As shown in panels a, b, and c of Figure 2, all MS of the isomers of $C_{12}H_{24}(CH_3S)_2$ show the diagnostic fragment ions $(A)^+ = m/z$ 159.1202 (base peak in the spectrum, $C_8H_{16}SCH_3$) and $(B)^+ = m/z$ 103.0576 ($C_4H_8SCH_3$), which indicate that all three isomers have the double bond between carbon 4 and 5. Based on all of the results described above, we confirm that D-3 is 4-dodecene and that D-1 and D-2 are 7-methylundec-4-ene. When these three dimers are compared to two 1-hexene molecules, the double bond between C1 and C2 in one molecule shifted to the position between C2 and C3 (C4 and C5 in the dimer), while the double bond in the other molecule was saturated after the addition reaction. This can be attributed to only the Alder-ene reaction between two hexene molecules. We propose the possible reaction pathways, as illustrated in Scheme 1. During the reaction, a new C−C bond forms between C1 of one 1-hexene molecule and C1′ or C2′ of a neighboring 1-hexene molecule. Concurrently, a hydrogen atom on C3 transfers to C2′ or C1′ via a six-membered ring transition state, resulting in the formation of 4-dodecene and 7-methylundec-4-ene.

https://doi.org/10.1021/acs.jpclett.4c03696
J. Phys. Chem. Lett. 2025, 16, 2445−2451

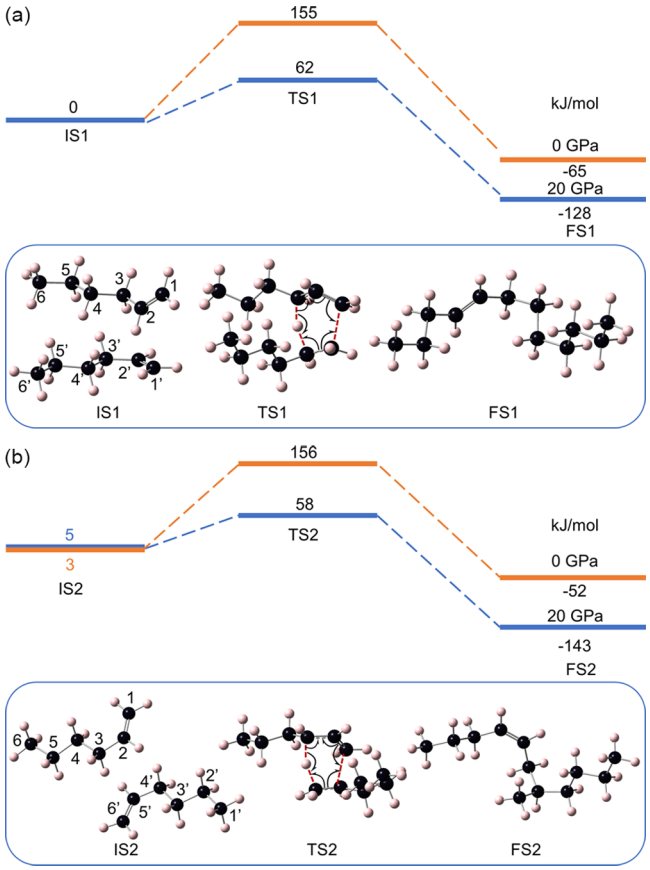

Figure 5. Gibbs free energy profile of reaction paths of 1-hexene. The formations of (a) 4-dodecene and (b) 7-methylundec-4-ene. Blue lines represent the potential energy profile corrected by $P\Delta V^{\ddagger}$, and $P\Delta V$ refers to the volume of IS. IS, initial state; TS, transition state, and FS, product. The unit of energy is kJ/mol. The energy of IS1 is used as the zero point.

Different from the reported Alder-ene reactions that take place in solution, this reaction is a solid-state Alder-ene reaction. Thus, molecular stacking plays an important role in understanding the reaction process. Based on this, *in situ* neutron diffraction of C_6D_{12} under high pressure was conducted up to 14 GPa to understand the high-pressure structural evolution of 1-hexene (Figure 3a). Liquid C_6D_{12} was cryogenically loaded into the PE press, and the pressure was quickly increased to 5.9 GPa to seal the sample. As the pressure increased, all diffraction peaks shifted toward lower d spacing, with no new peaks emerging up to 14 GPa. This suggests that 1-hexene does not undergo phase transition up to 14 GPa. The crystal structure of C_6D_{12} was then determined from the neutron diffraction spectra at 5.9 GPa using Topas software.[36] Initially, we constructed a rigid body model based on the molecular structure of 1-hexene. Rietveld refinement results (Figure 3b) show that the best fit is achieved when a *gauche* conformation was formed between C1 and C4, as shown in the inset of Figure 3b and Figure 4a. The obtained structure has a space group $P2_1/c$, with unit cell parameters a = 6.842 ± 0.001 Å, b = 15.663 ± 0.003 Å, c = 7.080 ± 0.001 Å, and β = 138.088 ± 0.009° at 5.9 GPa. Its lattice parameters decrease gradually with increasing pressure up to 14.0 GPa, as shown in Figure S5a of the Supporting Information. The pressure−volume ($P-V$) relationship of C_6D_{12} was fitted using the third-order Birch−Murnaghan equation of state, as shown in Figure S5b of the Supporting Information, with V_0 = 762 ± 40 Å^3, B_0 = 6.1 ± 1.2 GPa and B_1 fixed at 4. Subsequently, we optimized the structure of 1-hexene at 18 GPa by the Cambridge Sequential Total Energy Package (CASTEP) module in Materials Studio 2017 R2.[37] During this process, the unit cell parameters were fully relaxed to ensure that both the atomic positions and lattice dimensions were optimized. Then, the distances between the carbon atoms at the reaction sites were measured, which shows that the distance between C1 and C2′ is 4.13 Å, as shown in Figure 4b. This is significantly larger than the empirical shortest intermolecular C···C distance (2.8−3.4 Å) of the unsaturated compounds at the pressures before reactions.[38] For example, alkynes often polymerize when the minimum intermolecular C···C distance ($d_{(C\cdots C)min}$) reaches approximately 3 Å,[39,40] aromatics react at 2.8 Å,[41,42] and alkynylarenes react at 3.2−3.4 Å.[22,23] Consequently, we infer that 1-hexene under high pressure does not adhere to the principles governing topochemical polymerization and needs additional movement to reach the suitable position for the Alder-ene reaction.[43−46]

To further elucidate the high-pressure Alder-ene reaction of 1-hexene, the corresponding chemical reaction mechanism was then investigated by the density functional theory (DFT) calculation, as implemented in Gaussian. All of the calculations were done at the level of B3LYP/6-311g(d, p) with DFT-D3(BJ) correction to take the non-covalent effects into consideration. Frequency calculations were conducted to confirm the transition states (TS), and the intrinsic reaction coordinate (IRC) calculations for TS were subsequently performed to find the reaction mechanism, as shown by the orange line in Figure 5. The Cartesian coordinates for each structure are provided in Tables S3−S8 of the Supporting Information. As illustrated in panels a and b of Figure 5, two reaction routes were found that are consistent with our GC−MS results and confirm our proposed reactions in Scheme 1. The Alder-ene reaction starts with allylic C−H transferring to C2′ of the other molecule and experienced TS1 with an energy barrier of 155 kJ/mol per reaction (referring to the initial state 1, IS1) to form 4-dodecene (FS1). Another reaction route (route 2) contains a similar hydrogen transfer process to C1′ of the other 1-hexene with an energy barrier of 154 kJ/mol per reaction (referring to the initial state 2, IS2) to form 7-methylundec-4-ene. Both these reaction routes contain a six-membered ring transition state with one C−H σ bond and two alkene π bonds and are typical Alder-ene reactions.

To estimate the Gibbs free energy under high pressure, we incorporated the contribution of the PV term to G following Hoffmann's report.[21] The volume of activation ($\Delta V^{\ddagger} = V_{TS} - V_{IS}$) and the volume change for reaction ($\Delta V = V_{FS} - V_{IS}$) significantly affect the reaction, where IS, TS, and FS stand for the initial state, transition state, and final state. The value of $\Delta V^{\ddagger}$ was obtained using Multiwfn[47] software at 0 GPa, with molecular surfaces defined at the isosurfaces of charge density at 0.002 au (Table S9 of the Supporting Information).[48] At 20 GPa, the change of Gibbs free energy was corrected by $\Delta G^{\ddagger}(20\ \text{GPa}) = \Delta G^{\ddagger}(0\ \text{GPa}) + \int_{0\ \text{GPa}}^{20\ \text{GPa}} \Delta V^{\ddagger}\, dP$. If we use the average value of $\Delta V^{\ddagger}$ at 20 and 0 GPa to simulate the integral term, then we obtain $\Delta G^{\ddagger}(20\ \text{GPa}) = \Delta G^{\ddagger}(0\ \text{GPa}) + P(\Delta V^{\ddagger}(20\ \text{GPa}) + \Delta V^{\ddagger}(0\ \text{GPa}))/2$. Supposing that the TS and IS have a similar compressibility, that is, $V_{IS}(20\ \text{GPa})/V_{IS}(0\ \text{GPa}) = V_{TS}(20\ \text{GPa})/V_{TS}(0\ \text{GPa}) = \Delta V^{\ddagger}(20\ \text{GPa})/\Delta V^{\ddagger}(0\ \text{GPa})$, we can obtain $\Delta V^{\ddagger}(20\ \text{GPa}) = V_{IS}(20\ \text{GPa})/V_{IS}(0\ \text{GPa}) \times \Delta V^{\ddagger}(0\ \text{GPa})$. The ratio of $V_{IS}(20\ \text{GPa})/V_{IS}(0$

https://doi.org/10.1021/acs.jpclett.4c03696
J. Phys. Chem. Lett. 2025, 16, 2445−2451

GPa) was obtained from the experimental equation of state, that is, 0.48. When P = 20 GPa, $\Delta G^{\ddagger}$(20 GPa) is found to decrease to 62 kJ/mol for route 1 and 53 kJ/mol for route 2. Similarly, ΔG(20 GPa) = ΔG(0 GPa) + $P(\Delta V$(20 GPa) + ΔV(0 GPa))/2, and we can obtain ΔG(20 GPa) = −128 and −148 kJ/mol for routes 1 and 2, respectively. The overall energy profile is shown in Figure 5 (blue lines). The uncertainty of the energy value mainly comes from the estimation of V_{TS} and V_{FS} under high pressure. If $\Delta V^{\ddagger}$ did not change with pressure (overestimation), the $P\Delta V^{\ddagger}$ term would be as large as −126 and −138 kJ/mol and $\Delta G^{\ddagger}$(20 GPa) would be 29 and 16 kJ/mol for routes 1 and 2, respectively. If $\Delta V^{\ddagger}$ decreased to zero at 20 GPa (underestimation) and the average value of $\Delta V^{\ddagger}$ becomes $\Delta V^{\ddagger}$(0 GPa)/2, then the $P\Delta V^{\ddagger}$ term would be as small as −63 and −69 kJ/mol and $\Delta G^{\ddagger}$(20 GPa) would be 92 and 84 kJ/mol for routes 1 and 2, respectively. Because the compressibility of the TS is unknown, we can only make the above estimation. Nevertheless, the energy barrier of the Alder-ene reaction can be decreased obviously under high pressure and make the reaction feasible.

In summary, the solid-state Alder-ene reaction in 1-hexene under high-pressure and room-temperature conditions was confirmed by vibrational spectroscopy, high-resolution gas chromatography−mass spectrometry (HRGC−MS), *in situ* neutron diffraction, and a theoretical calculation. Allylic hydrogen from one 1-hexene shifted to C═C in the other molecule with a new C−C bond formation and double-bond migration. This reaction was evidenced to proceed to a six-electron cyclic transition state, which decreased obviously under high pressure. The *in situ* neutron diffraction shows that this reaction is not controlled by the topochemical process. This investigation presents a novel pathway for the realization of the Alder-ene reaction in the solid state and offers new insights into hydrogen transfer behavior in unsaturated hydrocarbons under high pressure.

■ ASSOCIATED CONTENT

Supporting Information

The Supporting Information is available free of charge at https://pubs.acs.org/doi/10.1021/acs.jpclett.4c03696.

Experimental procedures and calculation details as well as supplementary figures and tables, including the synthesis of sample PE-20, *in situ* high-pressure Raman spectroscopy, IR spectroscopy, HRGC−MS, and gas chromatography−quadrupole time-of-flight mass spectrometry (GC−Q/TOF-MS) experiments, and DFT calculations (PDF)

■ AUTHOR INFORMATION

Corresponding Author

Kuo Li − *Center for High Pressure Science and Technology Advanced Research, Beijing 100193, People's Republic of China;* orcid.org/0000-0002-4859-6099; Email: likuo@hpstar.ac.cn

Authors

Jingqin Xu − *Center for High Pressure Science and Technology Advanced Research, Beijing 100193, People's Republic of China*

Puyi Lang − *Center for High Pressure Science and Technology Advanced Research, Beijing 100193, People's Republic of China*

Shijie Liang − *Center for High Pressure Science and Technology Advanced Research, Beijing 100193, People's Republic of China*

Jie Zhang − *Center for High Pressure Science and Technology Advanced Research, Beijing 100193, People's Republic of China*

Yunfan Fei − *Center for High Pressure Science and Technology Advanced Research, Beijing 100193, People's Republic of China*

Yajie Wang − *Center for High Pressure Science and Technology Advanced Research, Beijing 100193, People's Republic of China*

Dexiang Gao − *Institute of High Energy Physics, Chinese Academy of Sciences, Beijing 100049, People's Republic of China; Spallation Neutron Source Science Center, Dongguan 523803, People's Republic of China*

Takanori Hattori − *J-PARC Center, Japan Atomic Energy Agency, Tokai, Ibaraki 319-1195, Japan*

Jun Abe − *Neutron Science and Technology Center, Comprehensive Research Organization for Science and Society, Tokai, Ibaraki 319-1106, Japan*

Xiao Dong − *Key Laboratory of Weak-Light Nonlinear Photonics, School of Physics, Nankai University, Tianjin 300071, People's Republic of China;* orcid.org/0000-0003-4533-1914

Haiyan Zheng − *Center for High Pressure Science and Technology Advanced Research, Beijing 100193, People's Republic of China;* orcid.org/0000-0002-4727-5912

Complete contact information is available at: https://pubs.acs.org/10.1021/acs.jpclett.4c03696

Notes

The authors declare no competing financial interest.

■ ACKNOWLEDGMENTS

This work was supported by the National Key Research and Development Program of China (2019YFA0708502). The authors acknowledge the support from the National Natural Science Foundation of China (NSFC, Grant 22022101). Neutron diffraction experiments at J-PARC were performed through the J-PARC user programs (2024A0062). The authors thank Dr. Zhe Cao and Kong Ye of Agilent Technologies (China), Inc. for their assistance in the GC−Q/TOF-MS experiment.

■ REFERENCES

(1) Treibs, W.; Schmidt, H. Zur katalytischen Dehydrierung hydroaromatischer Verbindungen. *Ber. Dtsch. Chem. Ges.* **1927**, *60*, 2335−2341.

(2) Alder, K.; Pascher, F.; Schmitz, A. Über die Anlagerung von Maleinsäure-anhydrid und Azodicarbonsäure-ester an einfach ungesättigte Koh an einfach ungesättigte Kohlenwasserstoffe. Zur Kenntnis von Substitutionsvorgängen in der Allyl-Stellung. *Ber. Dtsch. Chem. Ges.* **1943**, *76*, 27−53.

(3) Dubac, J.; Laporterie, A. Ene and retro-ene reactions in group 14 organometallic chemistry. *Chem. Rev.* **1987**, *87*, 319−334.

(4) Clarke, M. L.; France, M. B. The carbonyl ene reaction. *Tetrahedron* **2008**, *64*, 9003−9031.

(5) Xia, Q.; Ganem, B. Asymmetric total synthesis of (−)-α-kainic acid using an enantioselective, metal-promoted ene cyclization. *Org. Lett.* **2001**, *3*, 485−487.

(6) Zhang, J. H.; Wang, M. X.; Huang, Z. T. The aza-ene reaction of heterocyclic kentene aminals with enones: an unusual and efficient

formation of imidazo [1, 2-a] pyridine and imidazo [1, 2, 3-ij] [1, 8] naphthyridine derivatives. *Tetrahedron Lett.* **1998**, *39*, 9237−9240.
(7) Barriault, L.; Deon, D. H. Total synthesis of (+)-arteanniun M using the tandem oxy-cope/ene reaction. *Org. Lett.* **2001**, *3*, 1925−1927.
(8) Jin, R.; Liu, S.; Lan, Y. Distortion−interaction analysis along the reaction pathway to reveal the reactivity of the Alder-ene reaction of enes. *RSC Adv.* **2015**, *5*, 61426−61435.
(9) Gupta, S.; Lin, Y.; Xia, Y.; Wink, D. J.; Lee, D. Alder-ene reactions driven by high steric strain and bond angle distortion to form benzocyclobutenes. *Chem. Sci.* **2019**, *10*, 2212−2217.
(10) Hoffmann, H. The ene reaction. *Angew. Chem., Int. Ed.* **1969**, *8*, 556−577.
(11) Oppolzer, W.; Snieckus, V. Intramolecular ene reactions in organic synthesis. *Angew. Chem., Int. Ed.* **1978**, *17*, 476−486.
(12) Liu, X.; Zheng, K.; Feng, X. Advancements in catalytic asymmetric intermolecular ene-type reactions. *Synthesis* **2014**, *46*, 2241−2257.
(13) Hashmi, A. S. K.; Littmann, A. Gold catalysis: one-pot alkylideneoxazoline synthesis/Alder-ene reaction. *Chem. - Asian J.* **2012**, *7*, 1435−1442.
(14) Trost, B. M. Palladium-catalyzed cycloisomerizations of enynes and related reactions. *Acc. Chem. Res.* **1990**, *23*, 34−42.
(15) Trost, B. M.; Machacek, M. R.; Faulk, B. D. Sequential Ru−Pd catalysis: A two-catalyst one-pot protocol for the synthesis of N-and O-heterocycles. *J. Am. Chem. Soc.* **2006**, *128*, 6745−6754.
(16) Brummond, K. M.; You, L. Consecutive Rh (I)-catalyzed Alder-ene/Diels−Alder/Diels−Alder reaction sequence affording rapid entry to polycyclic compounds. *Tetrahedron* **2005**, *61*, 6180−6185.
(17) Chen, Z.; Liang, J.; Yin, J.; Yu, G. A.; Liu, S. H. Alder-ene reaction of aryne with olefins. *Tetrahedron Lett.* **2013**, *54*, 5785−5787.
(18) Pedrosa, R.; Andrés, C.; Martín, L.; Nieto, J.; Rosón, C. Diastereoselective intramolecular Alder-ene reaction on chiral perhydro-1, 3-benzoxazines. A rapid entry to enantiopure cis-3,4-disubstituted pyrrolidines. *J. Org. Chem.* **2005**, *70*, 4332−4337.
(19) Vo, D. V.; Su, S.; Karmakar, R.; Lee, D. Reactivity of enyne-allenes generated via an Alder-ene reaction. *Org. Lett.* **2024**, *26*, 1299−1303.
(20) Ohashi, M.; Jamieson, C. S.; Cai, Y.; Tan, D.; Kanayama, D.; Tang, M. C.; Anthony, S. M.; Chari, J. V.; Barber, J. S.; Picazo, E.; Kakule, T. B.; Cao, S.; Garg, N. K.; Zhou, J.; Houk, K. N.; Tang, Y. An enzymatic Alder-ene reaction. *Nature* **2020**, *586*, 64−69.
(21) Chen, B.; Hoffmann, R.; Cammi, R. The effect of pressure on organic reactions in fluids-a new theoretical perspective. *Angew. Chem. Int. Ed.* **2017**, *56*, 11126−11142.
(22) Li, Y.; Tang, X.; Zhang, P.; Wang, Y.; Yang, X.; Wang, X.; Li, K.; Wang, Y.; Wu, N.; Tang, M.; Xiang, J.; Lin, X.; Lee, H. H.; Dong, X.; Zheng, H.; Mao, H. K. Scalable high-pressure synthesis of sp^2-sp^3 carbon nanoribbon via [4 + 2] polymerization of 1,3,5-triethynylbenzene. *J. Phys. Chem. Lett.* **2021**, *12*, 7140−7145.
(23) Zhang, P.; Tang, X.; Wang, Y.; Wang, X.; Gao, D.; Li, Y.; Zheng, H.; Wang, Y.; Wang, X.; Fu, R.; Tang, M.; Ikeda, K.; Miao, P.; Hattori, T.; Sano-Furukawa, A.; Tulk, C. A.; Molaison, J. J.; Dong, X.; Li, K.; Ju, J.; Mao, H. K. Distance-selected topochemical dehydro-Diels-Alder reaction of 1,4-diphenylbutadiyne toward crystalline graphitic nanoribbons. *J. Am. Chem. Soc.* **2020**, *142*, 17662−17669.
(24) Zhang, P.; Gao, D.; Tang, X.; Yang, X.; Zheng, H.; Wang, Y.; Wang, X.; Xu, J.; Wang, Z.; Liu, J.; Wang, X.; Ju, J.; Tang, M.; Dong, X.; Li, K.; Mao, H. K. Ordered Van der Waals hetero-nanoribbon from pressure-induced topochemical polymerization of azobenzene. *J. Am. Chem. Soc.* **2023**, *145*, 6845−6852.
(25) Gao, D.; Tang, X.; Zhang, C.; Wang, Y.; Yang, X.; Zhang, P.; Wang, X.; Xu, J.; Su, J.; Liu, F.; Dong, X.; Lin, X.; Yuan, B.; Hiraoka, N.; Zheng, H.; Kang, L.; Li, K.; Mao, H.-k. Arylazo under extreme conditions: [2 + 2] cycloaddition and azo metathesis. *J. Phys. Chem. C* **2023**, *127*, 8482−8492.
(26) Huss, S.; Wu, S.; Chen, B.; Wang, T.; Gerthoffer, M. C.; Ryan, D. J.; Smith, S. E.; Crespi, V. H.; Badding, J. V.; Elacqua, E. Scalable synthesis of crystalline one-dimensional carbon nanothreads through modest-pressure polymerization of furan. *ACS Nano* **2021**, *15*, 4134−4143.
(27) Biswas, A.; Ward, M. D.; Wang, T.; Zhu, L.; Huang, H. T.; Badding, J. V.; Crespi, V. H.; Strobel, T. A. Evidence for orientational order in nanothreads derived from thiophene. *J. Phys. Chem. Lett.* **2019**, *10*, 7164−7171.
(28) Dunning, S. G.; Zhu, L.; Chen, B.; Chariton, S.; Prakapenka, V. B.; Somayazulu, M.; Strobel, T. A. Solid-state pathway control via reaction-directing heteroatoms: ordered pyridazine nanothreads through selective cycloaddition. *J. Am. Chem. Soc.* **2022**, *144*, 2073−2078.
(29) Wang, X.; Tang, X.; Yang, X.; Wang, Y.; Zhang, P.; Dong, X.; Yang, D.; Lü, X.; Zheng, H.; Li, K.; Mao, H. K. High-pressure synthesis of highly conjugated polymers via synergistic polymerization of phenylpropiolic acid. *ACS Appl. Polym. Mater.* **2022**, *4*, 5246−5252.
(30) Zhang, P.; Tang, X.; Zhang, C.; Gao, D.; Wang, X.; Wang, Y.; Guo, W.; Zou, R.; Han, Y.; Lin, X.; Dong, X.; Li, K.; Zheng, H.; Mao, H. K. Pressure-induced hydrogen transfer in 2-butyne via a double CH···π aromatic transition state. *J. Phys. Chem. Lett.* **2022**, *13*, 4170−4175.
(31) Shinozaki, A.; Kawano, J.; Nagai, T. Phase relation and reactivity of 1-hexene under high-pressure. *J. Phys. Chem. C* **2024**, *128*, 5956−5963.
(32) Schrötter, H. W.; Hoffmann, E. G. Raman-und Infrarot-Spektren einiger definiert an der doppelbindung deuterierter olefine. *Justus Liebigs Ann. Chem.* **1964**, *672*, 44−54.
(33) Han, J.; Tang, X.; Wang, Y.; Wang, Y.; Han, Y.; Lin, X.; Dong, X.; Lee, H. H.; Zheng, H.; Li, K.; Mao, H. K. Pressure-induced polymerization of monosodium acetylide: a radical reaction initiated topochemically. *J. Phys. Chem. C* **2019**, *123*, 30746−30753.
(34) Liao, S.; Sherman, G.; Huang, Y. Elucidation of double-bond positions of polyunsaturated alkenes through gas chromatography/mass spectrometry analysis of mono-dimethyl disulfide derivatives. *Rapid Commun. Mass Spectrom.* **2022**, *36*, No. e9228.
(35) Carlson, D. A.; Roan, C. S.; Yost, R. A.; Hector, J. Dimethyl disulfide derivatives of long chain alkenes, alkadienes, and alkatrienes for gas chromatography/mass spectrometry. *Anal. Chem.* **1989**, *61*, 1564−1571.
(36) Coelho, A. A. TOPAS and TOPAS-Academic: an optimization program integrating computer algebra and crystallographic objects written in C++. *J. Appl. Crystallogr.* **2018**, *51*, 210−218.
(37) Clark, S. J.; Segall, M. D.; Pickard, C. J.; Hasnip, P. J.; Probert, M. I.; Refson, K.; Payne, M. C. First principles methods using CASTEP. *Z. Kristallogr. Cryst. Mater.* **2005**, *220*, 567−570.
(38) Tang, X.; Dong, X.; Zhang, C.; Li, K.; Zheng, H.; Mao, H.-k. Triggering dynamics of acetylene topochemical polymerization. *Matter Radiat. Extremes* **2023**, *8*, No. 058402.
(39) Wang, X.; Tang, X.; Zhang, P.; Wang, Y.; Gao, D.; Liu, J.; Hui, K.; Wang, Y.; Dong, X.; Hattori, T.; Sano-Furukawa, A.; Ikeda, K.; Miao, P.; Lin, X.; Tang, M.; Zuo, Z.; Zheng, H.; Li, K.; Mao, H.-k. Crystalline fully carboxylated polyacetylene obtained under high pressure as a Li-ion battery anode material. *J. Phys. Chem. Lett.* **2021**, *12*, 12055−12061.
(40) Sun, J.; Dong, X.; Wang, Y.; Li, K.; Zheng, H.; Wang, L.; Cody, G. D.; Tulk, C. A.; Molaison, J. J.; Lin, X.; Meng, Y.; Jin, C.; Mao, H.-k. Pressure-induced polymerization of acetylene: structure-directed Stereoselectivity and a possible route to graphane. *Angew. Chem., Int. Ed.* **2017**, *56*, 6553−6557.
(41) Ciabini, L.; Santoro, M.; Gorelli, F. A.; Bini, R.; Schettino, V.; Raugei, S. Triggering dynamics of the high-pressure benzene amorphization. *Nat. Mater.* **2007**, *6*, 39−43.
(42) Wang, Y.; Dong, X.; Tang, X.; Zheng, H.; Li, K.; Lin, X.; Fang, L.; Sun, G.; Chen, X.; Xie, L.; Bull, C. L.; Funnell, N. P.; Hattori, T.; Sano-Furukawa, A.; Chen, J.; Hensley, D. K.; Cody, G. D.; Ren, Y.; Lee, H. H.; Mao, H.-k. Pressure-induced Diels−Alder reactions in C_6H_6-C_6F_6 cocrystal towards graphane structure. *Angew. Chem., Int. Ed.* **2019**, *58*, 1468−1473.
(43) Biradha, K.; Santra, R. Crystal engineering of topochemical solid state reactions. *Chem. Soc. Rev.* **2013**, *42*, 950−967.

https://doi.org/10.1021/acs.jpclett.4c03696
J. Phys. Chem. Lett. 2025, 16, 2445−2451

(44) Zhao, W.; Zhang, J.; Sun, Z.; Xiao, G.; Zheng, H.; Li, K.; Li, M.-R.; Zou, B. Chemical synthesis driven by high pressure. *CCS Chem.* **2025**, DOI: 10.31635/ccschem.024.202405293.
(45) Li, F.; Xu, J.; Wang, Y.; Zheng, H.; Li, K. Pressure-induced polymerization: addition and condensation reactions. *Molecules* **2021**, *26*, 7581.
(46) Yang, X.; Wang, X.; Wang, Y.; Li, K.; Zheng, H. From molecules to carbon materials—high pressure induced polymerization and bonding mechanisms of unsaturated compounds. *Crystals* **2019**, *9*, 490.
(47) Lu, T.; Chen, F. Multiwfn: a multifunctional wavefunction analyzer. *J. Comput. Chem.* **2012**, *33*, 580−592.
(48) Bader, R. F.; Carroll, M. T.; Cheeseman, J. R.; Chang, C. Properties of atoms in molecules: atomic volumes. *J. Am. Chem. Soc.* **1987**, *109*, 7968−7979.

https://doi.org/10.1021/acs.jpclett.4c03696
J. Phys. Chem. Lett. 2025, 16, 2445−2451